journal

J. Am. Ceram. Soc., 73 [4] 893–903 (1990)

Cyclic Fatigue-Crack Propagation in Magnesia-Partially-Stabilized Zirconia Ceramics

Reinhold H. Dauskardt,*,# David B. Marshall,*,† and Robert O. Ritchie#

Department of Materials Science and Mineral Engineering, University of California, Berkeley, California 94720; Center for Advanced Materials, Materials and Chemical Sciences Division, Lawrence Berkeley Laboratory, Berkeley, California 94720; and Rockwell International Science Center, Thousand Oaks, California 91360

The subcritical growth of fatigue cracks under (tension-tension) cyclic loading is demonstrated for ceramic materials, based on experiments using compact C(T) specimens of a MgO-partially-stabilized zirconia (PSZ), heat-treated to vary the fracture toughness K_c from ~3 to 16 MPa·m$^{1/2}$ and tested in inert and moist environments. Analogous to behavior in metals, cyclic fatigue-crack rates (over the range 10^{-11} to 10^{-5} m/cycle) are found to be a function of the stress-intensity range, environment, fracture toughness, and load ratio, and to show evidence of fatigue crack closure. Unlike toughness behavior, growth rates are not dependent on through-thickness constraint. Under variable-amplitude cyclic loading, crack-growth rates show transient accelerations following low–high block overloads and transient retardations following high–low block overloads or single tensile overloads, again analogous to behavior commonly observed in ductile metals. Cyclic crack-growth rates are observed at stress intensities as low as 50% of K_c, and are typically some 7 orders of magnitude faster than corresponding stress–corrosion crack-growth rates under sustained-loading conditions. Possible mechanisms for cyclic crack advance in ceramic materials are examined, and the practical implications of such "ceramic fatigue" are briefly discussed. [Key words: mechanical properties, zirconia: partially stabilized, magnesia, cracks, fatigue.]

I. Introduction

THE projected use of ceramics rather than metallic materials for structural applications has been motivated in part by the prospect that they may be insensitive to degradation from cyclic fatigue.[‡,1] However, several investigations[2–15] using smooth specimens, sometimes containing indentation flaws, tested under rotating bending, four-point bending, or by repeated thermal stressing, have shown reduced lifetimes for alumina, zirconia–alumina, TZP, and silicon nitride under cyclic, as opposed to static, loading conditions. Moreover, subcritical cracking has been reported for several monolithic and composite ceramics containing notches and tested under far-field cyclic compressive loads.[16–21] Here, limited crack extension occurs *from a notch* due to residual tensile stresses; mechanistically, it is still uncertain whether this process is similar to crack growth under applied tensile loads. However, there are few direct observations of fatigue crack growth in cyclic tension–tension loading in ceramics.

The refuted existence of true cyclic fatigue has been based primarily on the absence of crack-tip plasticity. However, other inelastic deformation mechanisms such as microcracking, martensitic transformation, or frictional sliding between a reinforcement phase and the matrix may exist in the vicinity of a crack tip. Direct evidence of cyclic fatigue-crack growth under tension–tension loads was first reported[22] in MgO-partially-stabilized zirconia (Mg-PSZ) that had been toughened slightly by martensitic transformation (fracture toughness, K_c = 5.5 MPa·m$^{1/2}$. Crack-growth rates were found to follow a power-law function of the stress-intensity range (with exponent ~24), were sensitive to frequency and load ratio, and exhibited crack closure, analogous to that in metals.[23] The existence of fatigue cracking under tension–tension loads was confirmed in Mg-PSZ[§] with higher toughness;[12,24] cyclic crack growth rates as a function of ΔK have also been reported for alumina under tension–compression loading.[25] Moreover, limited cyclic fatigue-crack growth data have been recently reported for several other ceramics, including alumina,[12,26] Si_3N_4,[26] SiC-reinforced alumina[27,28] and Y-TZP/Al_2O_3[29] composites, and pyrolytic carbon/graphite.[30]

In the present study, a more extensive examination of cyclic fatigue-crack growth in Mg-PSZ ceramics is undertaken to investigate the dependence of growth rate on (i) fracture toughness, (ii) the environment, (iii) through-thickness constraint, and (iv) variable-amplitude cyclic loading sequences (i.e., post-overload behavior). The results are compared with direct measurements of transformation zone characteristics in order to provide some elucidation of the mechanisms of cyclic fatigue.

II. Experimental Procedure

(1) Material

Precipitated, partially stabilized zirconia, containing 9 mol% magnesia (Mg-PSZ), was selected as the test material for its well-characterized and controllable transformation-toughening behavior.[31–35] The microstructure consists of cubic ZrO_2 grains, ~50 μm in diameter, with approximately 40 vol% lens-shaped tetragonal precipitates of maximum size 300 nm. The tetragonal phase undergoes a stress-induced martensitic transformation to a monoclinic phase in the presence of the high stress field near a crack tip. The resulting dilatant transformation zone in the wake of the crack exerts

A. Evans — contributing editor

Manuscript No. 198519. Received March 28, 1989; approved September 21, 1989.
Supported by the Office of Energy Research, Office of Basic Energy Sciences, Materials Sciences Division of the U.S. Department of Energy, under Contract No. DE-AC03-76F00098 at LBL, and by the U.S. Air Force Office of Scientific Research under Contract No. F49620-89-C-0031 at Rockwell.
*Member, American Ceramic Society.
#University of California and Lawrence Berkeley Laboratory.
†Rockwell International Science Center, Thousand Oaks, CA.
‡Although a redundant expression in metallurgical terminology, the term "*cyclic* fatigue" is used here to distinguish from other phenomena traditionally referred to in the ceramics literature as fatigue, i.e., static fatigue and dynamic fatigue.

§MS-grade Mg-PSZ, Nilcra Ceramics, Elmhurst, IL.

compressive tractions on the crack surfaces and hence shields¶ the crack tip from the applied (far-field) stresses.[36] The reduction in crack-tip stress-intensity factor, K_s, is dependent upon the volume fraction, f, of the transforming phase within the zone, the width w of the zone, and the dilational component of the transformation strain ε^T:[36–40]

$$K_{tip} = K - K_s \tag{1a}$$

where K_{tip} and K are the local (near-tip) and applied (far-field) stress-intensity factors, and

$$K_s \propto E'\varepsilon^T f w^{1/2} \tag{1b}$$

with $E' = E/(1 - \nu)$, E being Young's modulus and ν Poisson's ratio.

The Mg-PSZ was examined in four microstructural conditions, achieved by subeutectoid aging at 1100°C to vary the fracture toughness from 2.9 MPa·m$^{1/2}$ in the overaged (non-transformation-toughened) condition to 16 MPa·m$^{1/2}$ in the peak-toughened (TS) condition. The heat treatments, together with ambient-temperature mechanical properties, are listed in Table I. Further details of the microstructures and mechanical properties of these materials are described elsewhere.[32–35]

(2) Test Methods

(A) Cyclic Fatigue: Cyclic fatigue-crack propagation was measured using compact C(T) specimens, containing long (>3 mm) through-thickness cracks, in general accordance with the ASTM Standard E 647-86a for measurement of fatigue-crack growth rates in metallic materials.[44] Most test pieces were 3 mm in thickness, although thicknesses of 1.5 and 7.8 mm were also tested to examine the role of through-thickness constraint. Specimens were cyclically loaded at a load ratio (ratio of minimum to maximum loads) of 0.1 and a frequency of 50 Hz (sine wave) in high-resolution, computer-controlled electro-servo-hydraulic testing machines, operating under closed-loop displacement or stress-intensity control. Testing was performed in controlled room air (22°C, 45% rh), dehumidified gaseous nitrogen, and distilled water environments.

Electrical potential measurements across ~0.1-μm NiCr foils, evaporated onto the specimen surface, were used in situ to monitor crack lengths to a resolution better than ±2 μm.[22,45] Unloading compliance measurements using back-face gauges were also used to assess the extent of fatigue crack closure in terms of the far-field stress intensity, K_{cl}, at first contact of the fracture surfaces during the unloading cycle.[46] The K_{cl} value is calculated from the highest load where the elastic unloading compliance line deviates from linearity. However, it should be noted that for a transforming material such as PSZ, a local measure of the closure stress intensity will differ from the measured (far-field) value by an amount equal to the shielding stress intensity (Eq. (1a)). The test setup is illustrated in Fig. 1.

Crack-growth rates, da/dN, were determined over the range ~10^{-11} to 10^{-5} m/cycle under computer-controlled K-decreasing and K-increasing conditions. Data are presented in terms of the applied stress-intensity range ($\Delta K = K_{max} - K_{min}$, where K_{max} and K_{min} are the maximum and minimum stress intensities in the fatigue cycle). By considering the effect of crack closure, an effective (near-tip) stress-intensity range can also be estimated as $\Delta K_{eff} = K_{max} - K_{cl}$.

A fatigue threshold stress-intensity range, ΔK_{TH}, below which crack growth is presumed dormant,[47] was defined as the maximum value of ΔK at which growth rates did not exceed 10^{-10} m/cycle, consistent with the more conservative ASTM E 647 procedure.[44] Thresholds were approached by varying the applied loads so that the instantaneous values of crack length, a, and stress intensity range, ΔK, changed according to the equation[48]

$$\Delta K = \Delta K_0 \exp[C^*(a - a_0)] \tag{2}$$

where a_0 and ΔK_0 are the initial values of a and ΔK, and C^* is the normalized K-gradient $((1/K)(dK/da))$ which was set to ±0.08 mm^{-1}. For the C(T) geometry, stress intensities were computed from handbook solutions, in terms of the applied load P, crack length a, test-piece thickness B, and width W, as[49,50]

$$K = (P/BW^{1/2})g(a/W)$$

where

$$\begin{aligned} g(a/W) = \{&[2 + (a/W)][0.886 + 4.64(a/W) \\ &- 13.32(a/W)^2 + 14.72(a/W)^3 \\ &- 5.6(a/W)^4]\}/[1 - (a/W)]^{3/2} \end{aligned} \tag{3}$$

Owing to the brittleness of the materials, initiation of the precrack was one of the most critical procedures in the test. In the current work, as previously,[22,51] this was achieved by machining a wedge-shaped starter notch and carefully growing the crack roughly 2 mm out of this region by fatigue under displacement control. Thus, all measurements reported here involved cracks that had built up a wake of transformed material.

(B) Fracture Toughness: Following completion of the fatigue crack-growth tests, fracture toughnesses were determined by loading monotonically (with displacement control) to generate a resistance curve, $K_R(\Delta a)$. Procedures essentially conform to ASTM Standard E 399-87 for the measurement of the toughness at crack initiation, K_i.[52] In addition, a maximum toughness, K_c, was measured at the steady-state plateau or peak of the R-curve. Since these tests all involve sharp cracks, the measured toughnesses may be smaller than values obtained from other methods that rely on a machined notch as the initial crack.[30] On the other hand, test specimens that lead to instability of the crack in the rising part of the R-curve would give lower apparent toughnesses than those reported here.

III. Results and Discussion

(1) Role of Fracture Toughness

(A) Growth-Rate Behavior: Resistance curves for the four microstructures are illustrated in Fig. 2. The overaged material contains only transformed monoclinic precipitates and

¶Crack-tip shielding mechanisms act to impede crack advance by lowering the *local* "crack driving force" experienced in the vicinity of the crack tip (e.g., Ref. 23). Examples include transformation and microcrack toughening in ceramics (Refs. 31, 41), crack bridging in composites (Ref. 42) and crack closure during fatigue-crack growth (Ref. 43).

Table I. Heat Treatments and Tensile Properties of Mg-PSZ

Condition (grade)	Heat treatment	Young's modulus, E (GPa)	Approx. tensile strength (MPa)	Fracture toughness (MPa·m$^{1/2}$)* K_i	K_c
Overaged	24 h at 1100°C	<200	300	2.5	2.9
Low toughness (AF)	As received	208	300	3.0	5.5
Mid toughness (MS)	3 h at 1100°C	208	600	3.0	11.5
Peak toughness (TS)	7 h at 1100°C	208	400	3.5	16.0

*K_i and K_c are the initiation (from Ref. 35) and plateau toughness values from the R curve.

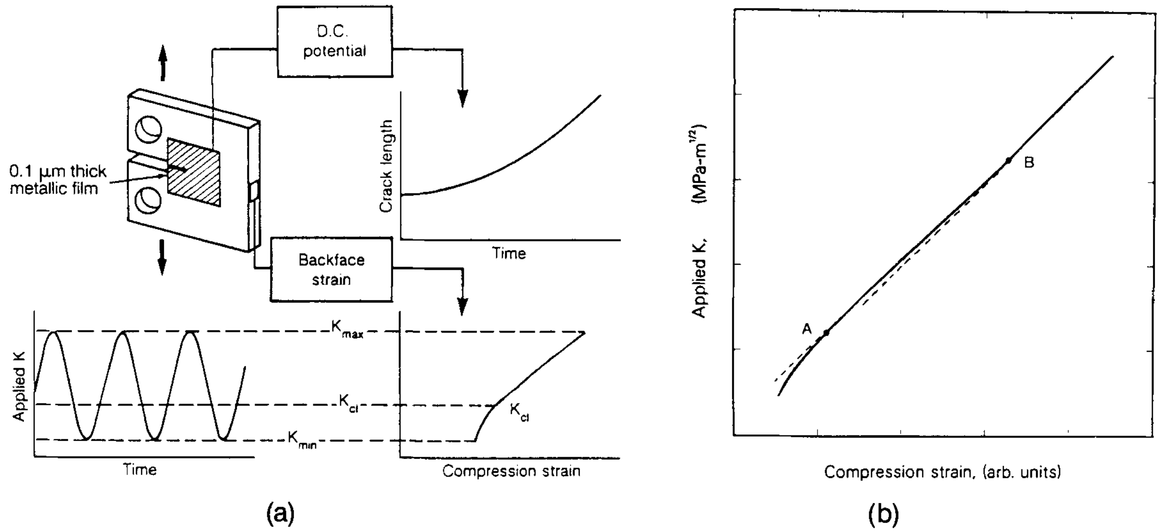

Fig. 1. Experimental techniques used to monitor continuously crack length and the stress intensity, K_{cl} at crack closure during cyclic fatigue-crack propagation tests are schematically illustrated in (a). Actual back-face strain data indicating points of marked (point A) and marginal (point B) deviations in linearity of the compliance curve are shown in (b).

shows only a very shallow R-curve with $K_c = 2.9$ MPa·m$^{1/2}$. The other materials exhibit various degrees of transformation toughening, with toughnesses (plateau K_c) of 5.5 to 16 MPa·m$^{1/2}$. Note that the results in Fig. 2 do not represent the entire R-curves, since measurements were obtained directly after fatigue testing, with the first measurement being taken at the K_{max} of the previous fatigue loading cycle.

Cyclic fatigue-crack propagation data are plotted in Fig. 3 as a function of the stress-intensity range ΔK, for a controlled room-air environment. As in metallic materials, growth rates can be fitted to a conventional Paris law relationship:[53]

$$da/dN = C(\Delta K)^m \tag{4}$$

However, the exponent m is considerably larger than reported for metals, i.e., in the range 21 to 42 (as opposed to 2 to 4 for metals), and the constant C scales inversely with the fracture toughness. It is especially noteworthy that the overaged material, in which the nonlinear deformation behavior associated with transformation plasticity has been removed, displays extensive cyclic fatigue-crack propagation, with a power-law dependence on the stress-intensity range similar to that of the toughened materials. Moreover, the present data indicate that the overaged material exhibits fatigue-crack growth at stress intensities below that required for crack initiation under monotonic loading on the R-curve (K_i values from Ref. 35 in Table I). In fact, each set of data shows an apparent threshold below which crack growth is presumed dormant (i.e., $<10^{-10}$ m/cycle) at a value, ΔK_{TH}, approximately 50% of K_c. Values of C, m, and ΔK_{TH} for each microstructure are listed in Table II. These results show that resistance to cyclic fatigue-crack growth in Mg-PSZ is enhanced with increasing fracture toughness.

The data in Fig. 3 for the low-toughness (AF) material were shown previously[22] to be a true cyclic fatigue phenomenon, with growth rates proportional to the *range* of stress intensity, rather than subcritical cracking at maximum load. These tests involved monitoring crack growth rates at constant K_{max}, with (i) the load cycled between K_{max} and K_{min} ($R = 0.1$) compared to being held constant at K_{max} (Fig. 4(a)), and (ii) the value of K_{min} being varied (Fig. 4(b)).

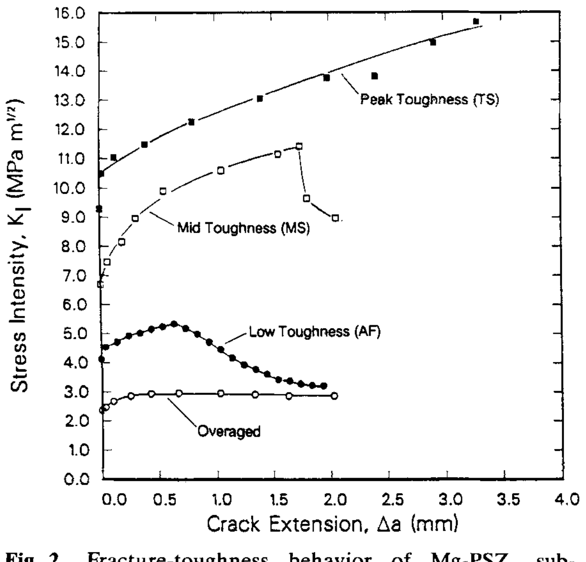

Fig. 2. Fracture-toughness behavior of Mg-PSZ, subeutectoid aged to a range of K_c values from 2.9 to 15.5 MPa·m$^{1/2}$, showing $K_R(\Delta a)$ resistance curves.

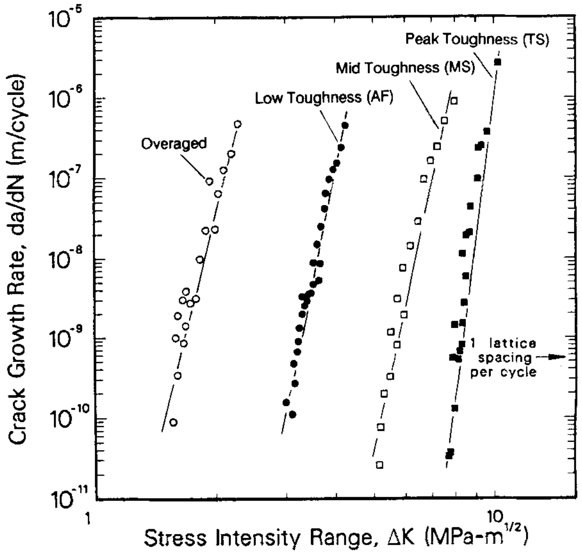

Fig. 3. Cyclic fatigue-crack growth behavior, in terms of growth rates per cycle, da/dN, as a function of the stress-intensity range, ΔK, for Mg-PSZ, subeutectoid aged to a range of K_c toughnesses from 2.9 to 15.5 MPa·m$^{1/2}$ Data were obtained on C(T) samples in a room-air environment at 50 Hz frequency with a load ratio ($R = K_{min}/K_{max}$) of 0.1.

Table II. Values of C and m (in Eq. (4)) and the Threshold ΔK_{TH} in Mg-PSZ

	K_c (MPa·m$^{1/2}$)	C (m/cycle (MPa·m$^{1/2}$)$^{-m}$)	m	ΔK_{TH}* (MPa·m$^{1/2}$)
Overaged	2.9	2.00×10^{-14}	21	1.6
Low toughness (AF)	5.5	4.89×10^{-22}	24	3.0
Mid toughness (MS)	11.5	5.70×10^{-28}	24	5.2
Peak toughness (TS)	16.0	1.70×10^{-48}	42	7.7

*ΔK_{TH} defined at a maximum growth rate less than 10^{-10} m/cycle.[47]

(B) Fractography: The transgranular nature of crack paths was clearly evident from optical microscopy of etched surfaces (Fig. 5) in which grain boundaries were decorated with monoclinic zirconia phase. Crack paths additionally show evidence of frequent crack deflection, branching, and uncracked ligament bridging behind the crack tip. The degree of crack tortuosity, however, appears progressively diminished with decreasing toughness, as evidenced by the comparatively flat crack path in the overaged microstructure (Fig. 5(b)). Corresponding scanning electron micrographs (Fig. 6) indicate that the fracture-surface appearance under cyclic loading is nominally identical to that under monotonic loading; moreover, unlike many metals and polymers, no evidence of fatigue striations or crack arrest markings are apparent on the fatigue fracture surfaces.[††]

(C) Fatigue Crack Closure: In addition to possible crack-tip shielding from crack deflection and bridging noted above, fatigue-crack growth in PSZ ceramics shows evidence of crack closure, analogous to behavior in metals.[23,43,54] Such closure involves premature contact between the crack surfaces during the unloading cycle, which raises the effective K_{min} ($\equiv K_{cl}$), thereby lowering the effective ΔK.[54] Global (far-field) K_{cl} values, calculated from the highest load at the onset of marked deviation from linearity of the back-face strain compliance measurements (point (A) in Fig. 1(b)), show increasing K_{cl}/K_{max} ratios as the threshold ΔK_{TH} is approached (Fig. 7), characteristic of (contact) shielding by wedging (which is enhanced at smaller crack opening displacements). In view of the deflected nature of the crack paths, it is suggested that such closure results primarily from the wedging action of fracture-surface asperities (roughness-induced crack closure).[55–57] This would also be consistent with the progressively higher levels of crack closure seen in the higher toughness microstructures, which exhibit the roughest crack paths. Moreover, the increasingly dilatant transformation zones in the tougher materials act to reduce the crack opening displacements, which further encourages premature crack-surface contact on unloading.

(D) Observation of Transformation Zones: The influence of transformation-zone shielding on fatigue cracking was investigated by comparing wake zones in the mid- and peak-toughened materials. Two techniques were used to characterize the zones: interference microscopy and Raman spectroscopy. The Raman spectroscopy provides a direct measure of the fraction of tetragonal and monoclinic phases within the zone, with a spatial resolution of ~2 μm (using a microprobe system).[58–60] The optical interference measurements from the polished face of the compact tension specimens provide a measure of normal surface displacements due to the transformation within the zone. The displacements are dependent on both the fraction of transformation and the net transformation strain.[59,61]

Raman measurements of the volume fraction of material transformed to the monoclinic phase, within zones adjacent to cracks that had been grown under cyclic loading at constant ΔK or under steady-state, monotonic loading (i.e., at $K = K_c$), are shown in Fig. 8. The results indicate that the fraction of transformed material is in all cases nonuniform and smaller than the total available fraction of tetragonal phase (~0.4), even adjacent to the fracture surface.

The shielding stress-intensity factors, K_s, corresponding to the data of Fig. 8 can be calculated by integration of Eq. (1*b*) (which is valid for a step-function zone profile):[‡‡]

[††]Similar results have been obtained in graphite/pyrolytic carbon laminates, where cyclic fatigue fracture morphologies are also indistinguishable from those of monotonic overload fractures (Ref. 30).

[‡‡]Integration of Eq. (1*b*) to obtain Eq. (5) requires that all contours of constant f in the wake and around the tip of the crack be geometrically similar. Other Raman measurements confirm that this requirement is satisfied.[59,60]

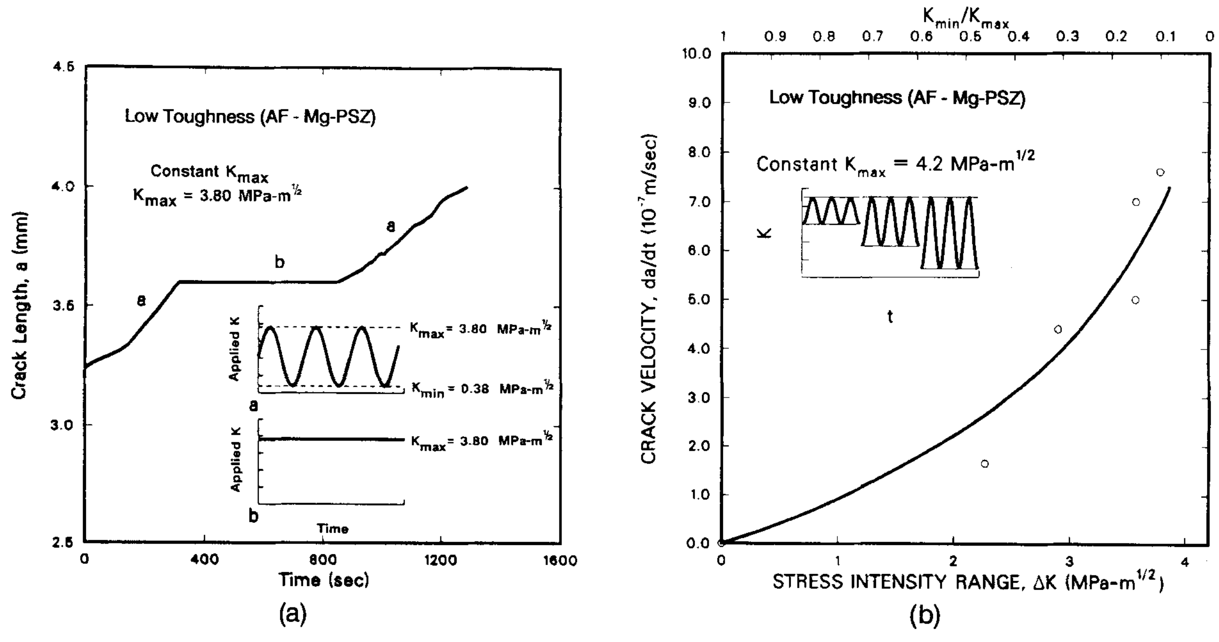

Fig. 4. Effect in low-toughness Mg-PSZ (AF) microstructure of (a) sustained and cyclic loading conditions on the crack velocity, da/dt, at constant K_{max} (=3.8 MPa·m$^{1/2}$), and (b) varying applied stress-intensity range ΔK on crack velocity at constant K_{max} (=4.2 MPa·m$^{1/2}$) [after Ref. 22].

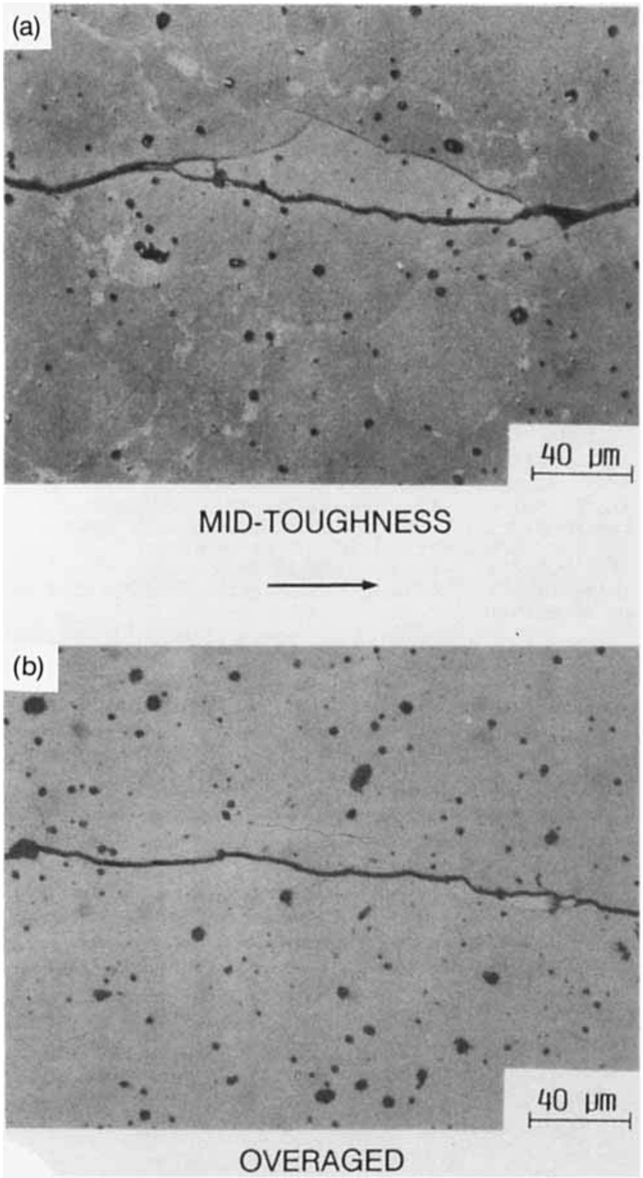

Fig. 5. Optical micrographs of the morphology of cyclic fatigue-crack paths in Mg-PSZ, showing (a) an increasingly deflected crack path in the mid-toughened (MS) microstructure at $\Delta K \sim 6$ MPa·m$^{1/2}$ compared to (b) an essentially linear crack path in the overaged material at $\Delta K \sim 2$ MPa·m$^{1/2}$. Note the transgranular fracture morphology and evidence of crack branching in the MS microstructure. Arrow indicates general direction of crack growth.

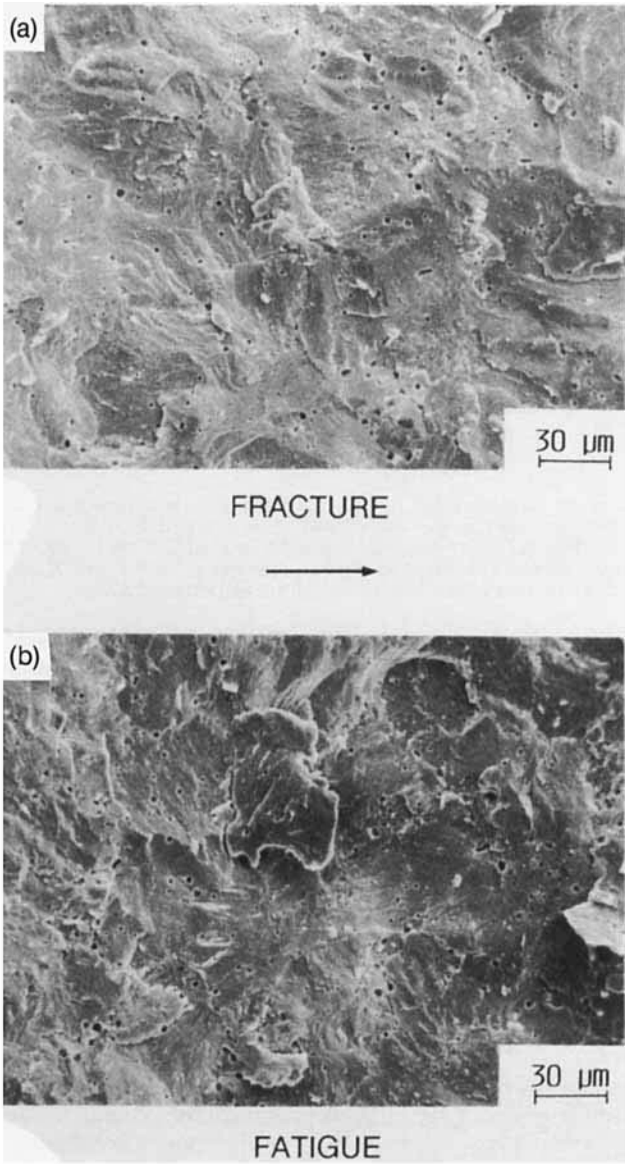

Fig. 6. Representative scanning electron micrographs of the nominally identical fracture-surface morphologies obtained in Mg-PSZ (MS grade) for (a) overload fracture under monotonic loads at $\Delta K \sim 11.5$ MPa·m$^{1/2}$, and (b) fatigue fracture under cyclic loads at $\Delta K \sim 6$ MPa·m$^{1/2}$. Note, in contrast to metals, the absence of striations or crack-arrest markings on the fatigue fracture surface. Arrow indicates general direction of crack growth.

$$K_s = AE'\varepsilon^T \int_0^w \frac{f}{2\sqrt{x}}\,dx \tag{5}$$

where the constant A is dependent upon the shape of the zone ahead of the crack tip as well as the transformation strain ε^T.[38] For a purely dilational transformation strain (i.e., all long-range shear strains relieved by twinning) and a frontal zone defined by a contour of constant hydrostatic stress in the crack-tip field, A is equal to 0.22.[36] The values of K_s evaluated from the four sets of data in Fig. 8, using Eq. (5) with $E' = E/(1-\nu) = 272$ MPa and $\varepsilon^T = 0.04$, are compared by plotting K_s as a function of the maximum *applied* stress intensity factor, K (K_{max} for cyclic loading, K for monotonic loading), in Fig. 9. For each material, the values of K_s under monotonic and cyclic loading conditions are consistent with the relation $K_s \propto K$ expected from Eq. (1*b*).[‡‡] Therefore, if the frontal zone shapes and the transformation strains ε^T are the same in cyclic and monotonic loading, the micromechanisms of fatigue-crack advance clearly do not involve a reduction in transformation-zone shielding.

A comparative assessment of the transformation strains in monotonic and fatigue loading can be obtained from optical interference measurements of the surface uplift at the locations from which the Raman data of Fig. 8 were obtained. The results plotted in Fig. 10 show differences between the four locations qualitatively similar to those of the Raman data. Comparison of the measured displacement, u_0, adjacent to the cracks with the values of K_s calculated from the Raman data, is shown in Fig. 11. Both u_0 and K_s must increase with increasing f and zone width. However, the measured values of u_0 are dependent on the transformation strains, ε^T, whereas a constant value of ε^T was assumed in calculating K_s. Therefore, the data in Fig. 11 would fall on different curves for cyclic and monotonic loading if the transformation strains differed for these two loading conditions (e.g., different amounts

[‡‡]Stresses outside the transformation zone are defined approximately by the applied stress intensity factor; $\sigma_{ij} \propto K/r^{1/2}$. Therefore, if the transformation occurs at a critical stress σ_c in a given material, then the zone width is $w \propto K^2$ and Eq. (1b) becomes $K_s \propto K$ (Ref. 62).

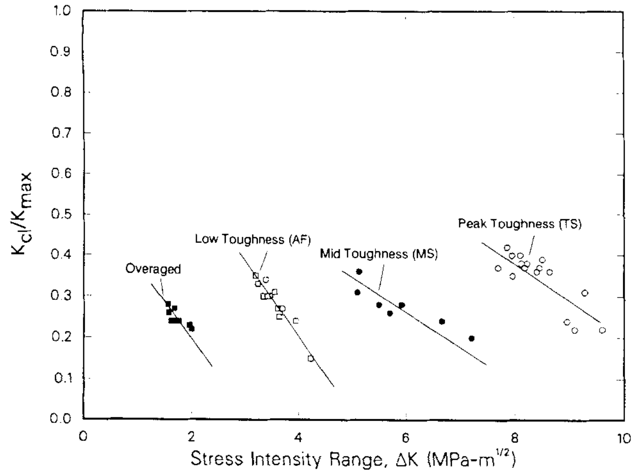

Fig. 7. Experimentally measured variation in fatigue crack closure corresponding to cyclic crack-growth rate data at $R = 0.1$, for the Mg-PSZ microstructures plotted in Fig. 3. Results, based on back-face strain compliance measurements, show the ratio K_{cl}/K_{max} as a function of the applied stress-intensity range, ΔK.

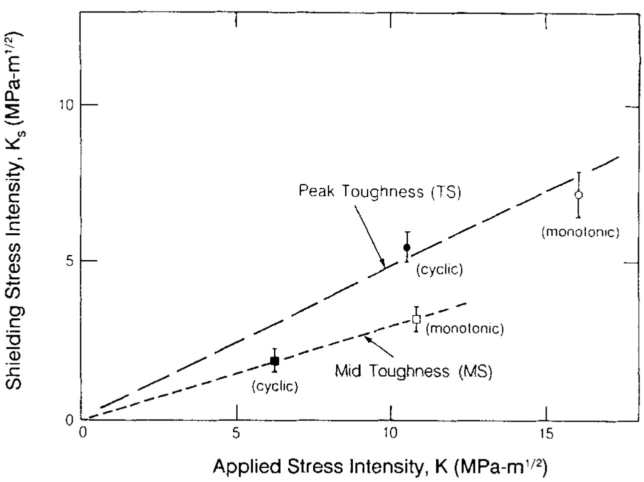

Fig. 9. Estimates of the shielding stress-intensity factor, K_s, calculated from Eq. (5) for the transformation zones presented in Fig. 8, as a function of the applied stress-intensity factor, K. Values of K_s under both monotonic and cyclic loading are consistent with the relation $K_s = \beta K$, where the slope of the curve β is dependent on the material.

of twinning resulting in different shear components in ε^T). Since all of the data fall on a single curve within the measurement accuracy, it is concluded that the *transformation strains*, in cyclic and monotonic loading *do not differ* significantly.

(2) *Role of Environment*

It has been suggested that cyclic fatigue effects in ceramics may be the result of stress–corrosion cracking.[1,7,63,64] To examine this hypothesis, cyclic crack-growth rates in the low-toughness AF material were measured in inert (dehumidified nitrogen gas) and corrosive (distilled water) environments; results are plotted as a function of ΔK in Fig. 12. Growth rates are faster in moist room air and water than in inert nitrogen, indicating a marked corrosion-fatigue effect which presumably involves the weakening of atomic bonds at the crack tip by the adsorption of water molecules. However, crack growth is observed in the inert atmosphere, implying that, analogous to behavior in metals and consistent with the observations cited above, *cyclic fatigue in the ceramic is a mechanically induced cyclic process which may be accelerated by the environment.*

Another comparison of the effects of mechanical load cycling and environmentally assisted crack growth is illustrated in Fig. 13 for the MS material tested in moist air. Cyclic crack velocities, expressed in terms of time (da/dt), are compared with corresponding stress–corrosion crack velocities measured under sustained loads; at equivalent K levels at this frequency, cyclic crack-growth rates are up to 7 orders of magnitude faster (or at equivalent velocities, K_{max} is smaller by about 40% for cyclic loading).

It would thus appear that nonconservative estimates of the subcritical advance of incipient cracks, and serious overestimates of lifetimes, may result if defect-tolerant predictions are based solely on sustained-load (stress–corrosion) and fracture-toughness data and do not consider a cyclic fatigue effect.

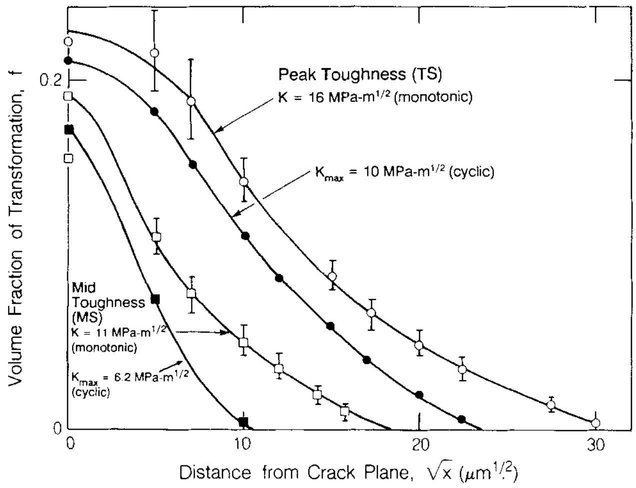

Fig. 8. Raman measurements of volume of material transformed from tetragonal to monoclinic phase in zones adjacent to cracks grown under both monotonic and cyclic loading conditions in the mid- (MS) and peak- (TS) toughened materials, as a function of distance x from the crack plane.

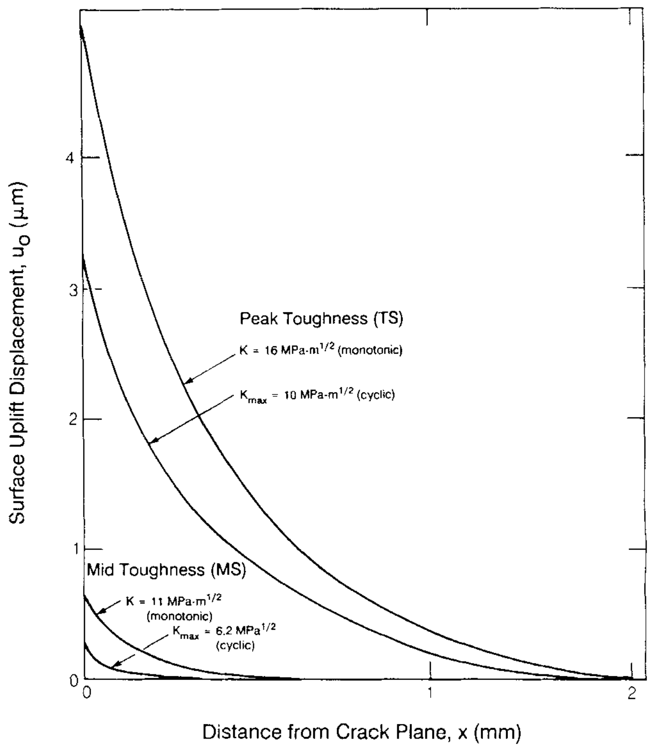

Fig. 10. Variation in surface uplift displacement, u_0, adjacent to cracks as calculated from optical interference measurements, showing qualitatively similar differences between the four locations assessed using Raman spectroscopy shown in Fig. 8.

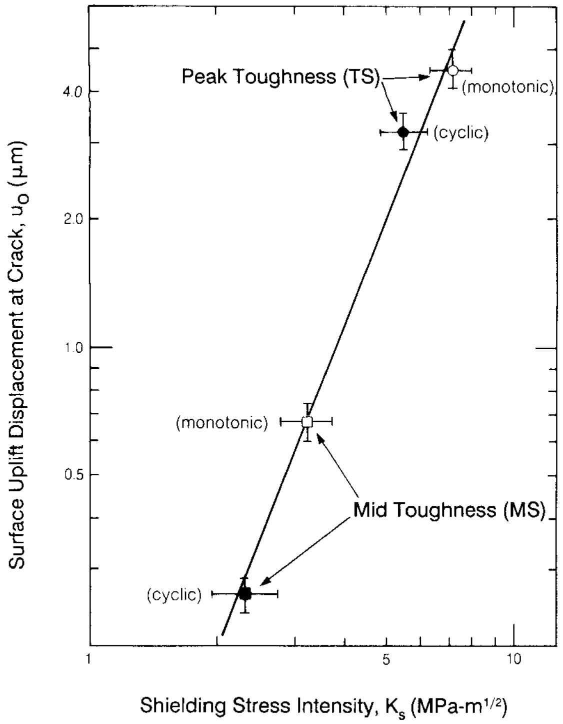

Fig. 11. Comparison of the surface uplift displacements, u_0, immediately adjacent cracks, with the values of K_s calculated from the Raman data, for cracks grown under monotonic and cyclic loading conditions. The resulting linear relationship implies that the transformation strains under cyclic and monotonic loading do not differ significantly.

(3) *Role of Through-Thickness Constraint*

Recent work[65] on R-curve behavior in Mg-PSZ has indicated an important effect of test-piece thickness on the fracture toughness. Specifically, the plateau toughness was 22% higher and the slope of the R-curve steeper in samples with a thickness of 4 mm compared to 1 mm. This trend is opposite to that accompanying the transition from plane stress to plane strain in metals, where the toughness decreases with increasing thickness, but is consistent with expectations for shielding due to transformation.

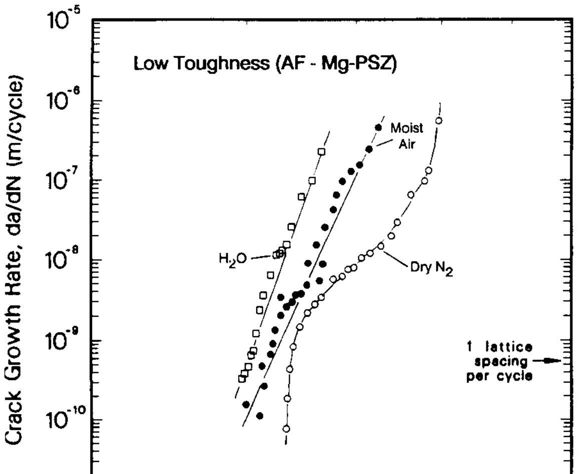

Fig. 12. Cyclic fatigue-crack growth rates, da/dN, as a function of the applied stress-intensity range, ΔK, in low-toughness (AF) Mg-PSZ in dry nitrogen gas, room air, and distilled water environments, showing an acceleration in growth rates due to water vapor. C(T) tests were performed at 50 Hz frequency with a load ratio R of 0.1.

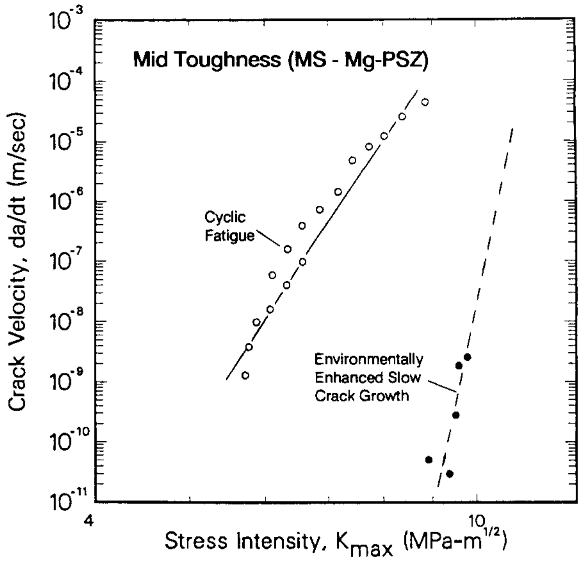

Fig. 13. Subcritical crack-growth behavior in mid-toughness (MS) Mg-PSZ, showing a comparison of crack velocities da/dt, as a function of K_{max}, measured under monotonic and cyclic loading conditions in a moist air environment. Note how the cyclic crack velocities are up to 7 orders of magnitude faster at equivalent stress-intensity levels.

To examine whether such through-thickness constraint effects are important in influencing fatigue behavior, cyclic fatigue-crack growth rates and R-curves were measured using C(T) specimens of the TS-grade material[§§] with thicknesses of 1.5 and 7.8 mm (Fig. 14). The K_c fracture-toughness values are larger in the thicker specimens by approximately 9% (Fig. 14(a)). However, no significant difference in the corresponding fatigue-crack propagation rates was detected (Fig. 14(b)).

(4) *Role of Variable-Amplitude Loading*

The results described above pertain to constant-amplitude cyclic loading; to examine the influence of variable-amplitude loading, single and block overload sequences were applied during steady-state fatigue-crack growth in the MS- and TS-grade materials. Results for high–low and low–high block overloads in mid-toughness (MS) material are shown in Fig. 15. Over the first ~2.5 mm of crack advance, the crack-growth rate remains approximately constant at constant $\Delta K(=5.48\ \mathrm{MPa \cdot m^{1/2}})$. On reducing the cyclic loads so that $\Delta K = 5.30\ \mathrm{MPa \cdot m^{1/2}}$ (high–low block overload), a transient retardation is seen followed by a gradual increase in growth rates until the (new) steady-state velocity is achieved. Similarly, by subsequently increasing the cyclic loads so that $\Delta K = 5.60\ \mathrm{MPa \cdot m^{1/2}}$ (low–high block overload), growth rates show a transient acceleration before decaying to the steady-state velocity. Such behavior is analogous to that widely observed in metals,[66] where to the first order the crack-growth increment affected by the overload is comparable with the extent of the overload plastic zone. In the present experiments, the affected crack-growth increments are ~500 μm, approximately 5 times the measured[59,60] transformed zone width of ~85 to 108 μm. This is consistent with zone-shielding calculations in which the maximum steady-state shielding is achieved after crack extensions of approximately 5 times the zone width.[36,37]

Similar crack-growth retardation following a high–low block overload ($\Delta K = 9.5$ to $8.5\ \mathrm{MPa \cdot m^{1/2}}$) is shown for

[§§]As TS-grade materials are prone to age at room temperature, resulting in lower toughness, tests on these two thicknesses were conducted at a nominally fixed period of time (approximately 1 month) following heat treatment.

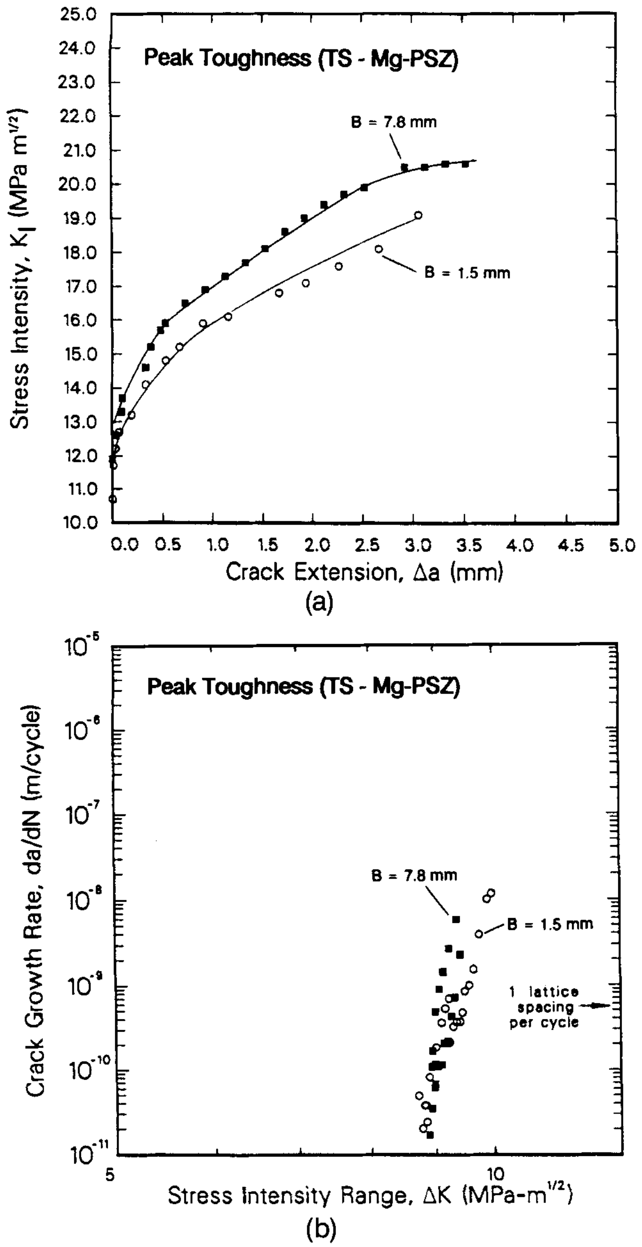

Fig. 14. Effect of through-thickness constraint on (a) $K_R(\Delta a)$ fracture-toughness resistance curves and (b) cyclic fatigue-crack propagation behavior in high-toughness (TS) Mg-PSZ, tested in a room-air environment. Note the higher toughness, yet relatively unaffected crack-growth rates, in the 7.8-mm-thick C(T) sample, compared to the 1.5-mm-thick sample.

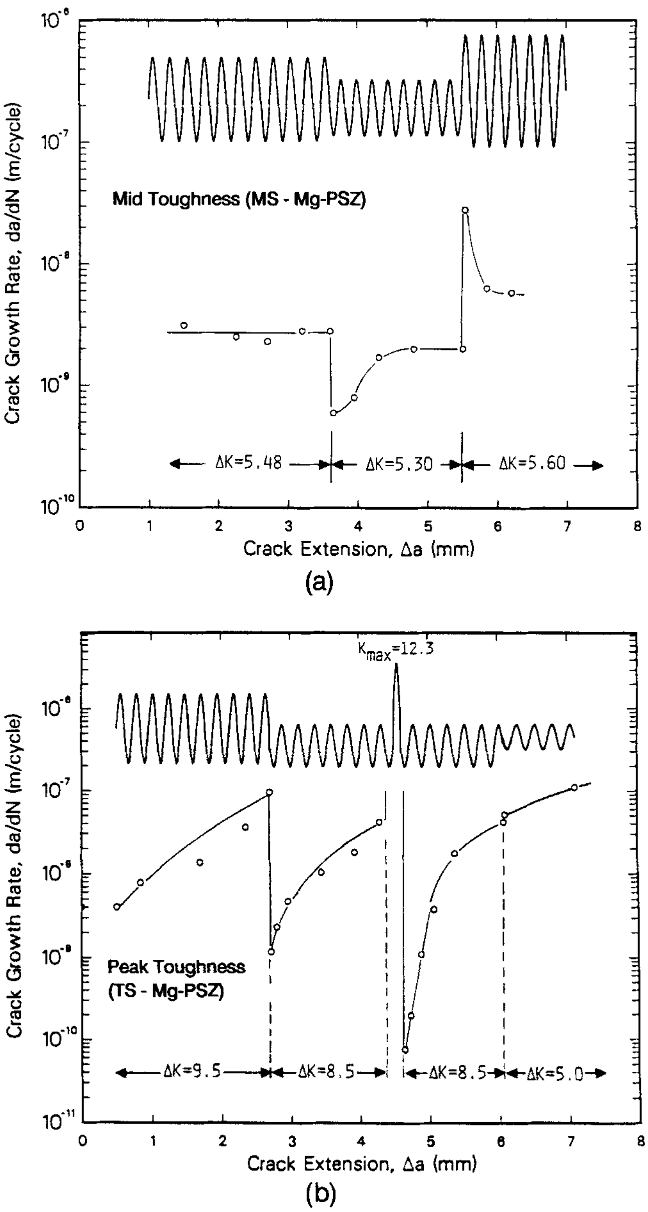

Fig. 15. Transient fatigue-crack growth behavior in (a) mid-toughness (MS) and (b) peak-toughness (TS) Mg-PSZ due to variable-amplitude cyclic loads, showing immediate crack-growth retardations following high–low block overloads, immediate accelerations following low–high block overloads, and delayed retardation following a single tensile overload.

peak-toughness Mg-PSZ in Fig. 15(b); in addition, significant retardation can be seen following a single tensile overload to a K_{max} of 12.3 MPa·m$^{1/2}$. Such results can be rationalized in terms of changes in crack-tip shielding from the transformation zone.[67]

IV. Mechanisms of Cyclic Fatigue

Mechanisms of fatigue crack growth may be conveniently classified into two categories; *intrinsic* mechanisms where the unloading portion of the cycle results in enhanced microstructural "damage" ahead of the crack tip (as in metals), and *extrinsic* mechanisms where the unloading acts to diminish the effect of a crack-tip shielding process, thereby increasing the near-tip stress intensity compared to equivalent monotonic loading conditions. In transforming ceramics, such an extrinsic mechanism could result from a reduction of the degree of transformation toughening under cyclic loading, resulting from changes in the process-zone morphology, cyclic accommodation of the transformation strains (related to the type of martensitic twin variants that form), or changes in the degree of reversibility of the transformation. Alternatively, if bridging by frictional/geometrical interlocking of microstructurally rough fracture surfaces[68,69] contributes significantly to the toughness, cyclic loading may result in progressive degradation of the bridging zone.

In the present study, however, several observations argue against such mechanisms, and suggest instead that an intrinsic mechanism is responsible for fatigue-crack growth in Mg-PSZ. The most compelling evidence is that crack growth under cyclic loading is exhibited by the overaged material in which stress-induced transformation cannot occur. Moreover, the crack-growth rates in all the materials can be shown to be uniquely related to the local (near-tip) stress-intensity range, ΔK_{tip}, regardless of the degree of transformation toughening. Evaluation of ΔK_{tip} must include the effects of both zone shielding and premature crack closure due to contact of asperities.[¶¶] The maximum and minimum near-tip stress-intensity factors are related to the corresponding far-field applied (measured) values, K_{max} and K_{cl} (using Eq. (1*a*)):

$$(K_{\text{tip}})_{max} = K_{max} - K_s \quad (6)$$

$$(K_{\text{tip}})_{min} = K_{cl} - K_s \quad (7)$$

K_s is assumed to remain constant during unloading and was shown in Section III(1) to be given by

$$K_s = \beta K_{max} \quad (8)$$

where β is a constant for a given material.

Equation (7) requires $K_{cl} \geq K_s$, that is, in the absence of roughness-induced closure, the transformation shielding causes crack-tip closure at $K_{cl} = K_s$, whereas the presence of sufficiently large roughness effects could cause contact behind the crack tip at larger values of K_{cl}. However, the closure stress intensity factors from Fig. 7 (measured from point (A) of the compliance curve of Fig. 1(b)) are smaller than the corresponding values of K_s in Fig. 9. This suggests that the values in Fig. 7 represent roughness-induced contact well behind the crack tip, at a lower applied load than that which allows initial, near-tip closure. Closer examination of the present unloading compliance curves reveals a marginal change in linearity after unloading ~20% to 30% from the maximum load (point (B) in Fig. 1(b)). Such behavior is consistent with the notion that, during unloading, crack-surface contact occurs first over a short distance (of the order of micrometers) behind the crack tip,[†††] before roughness-induced crack contact over the remaining crack surfaces. Estimation of the closure stress intensities from these higher closure loads yields K_{cl} values within 5% of K_s. Therefore, it appears that initial tip closure occurs at $K_{cl} = K_s$ and the tip-stress intensity range is given by

$$\Delta K_{\text{tip}} = K_{max} - K_s \quad (9)$$

The crack-growth rates for all materials are plotted in Fig. 16(a) in terms of ΔK_{tip} evaluated from Eq. (9), with K_s obtained from Eq. (8). All data fall close to a universal curve of the form

$$da/dN = A(\Delta K_{\text{tip}})^n \quad (10)$$

where $n = 22$ and $A = 3.5 \times 10^{-15}\ \text{m}^{(1-n/2)} \cdot \text{cycle}^{-1} \cdot \text{MPa}^{-n}$.

The growth-rate data may be normalized equivalently in terms of the steady-state toughness, K_c. This may be readily demonstrated by noting that $K_c = K_0 + K_s$, where K_0 is the intrinsic toughness (without transformation shielding), from which $K_c = K_0/(1 - \beta)$ from Eq. (8). With this result, Eq. (9) can be written

$$\Delta K_{\text{tip}} = K_0\left(\frac{K_{max}}{K_c}\right) \quad (11a)$$

or

$$\Delta K_{\text{tip}} = \frac{K_0}{(1 - R)}\left(\frac{\Delta K}{K_c}\right) \quad (11b)$$

where $\Delta K = K_{max}(1 - R)$, and Eq. (11) becomes

$$\frac{da}{dN} = A\frac{K_0^n}{(1 - R)^n}\left(\frac{\Delta K}{K_c}\right)^n \quad (12)$$

According to Eq. (12), a universal curve is obtained by shifting the data for each material in Fig. 3 along the ΔK axis by a constant multiplying factor, $K_0/[K_c(1 - R)]$. The result of normalizing the data in this manner is shown in Fig. 16(b). An analogous result for environmentally assisted crack growth has been discussed by Lawn.[70]

The Raman and surface-uplift measurements of Section III further support the contention that transformation-zone shielding is not affected by the cyclic nature of the loading. Specifically, the results in Figs. 9 and 11 indicate that for steady-state crack growth under cyclic or monotonic loading, K_s is determined by the maximum applied stress-intensity factor (Eq. (7)). Although these results pertain only to the contribution to K_s from the wake region of the zone (detailed comparisons of frontal zones have not yet been completed), preliminary estimates indicate that the frontal zone in fatigue loading would need to be enlarged by a factor of 4 compared with that in monotonic loading in order to make a significant difference to the above conclusions.

Potential intrinsic mechansims of fatigue include accumulated damage in material ahead of the crack tip in the form of localized microplasticity, or microcracking, particularly in grain boundary and precipitate/matrix interface regions. Matrix microcracking associated with the formation of transformation shear bands has also been suggested.[21] Such

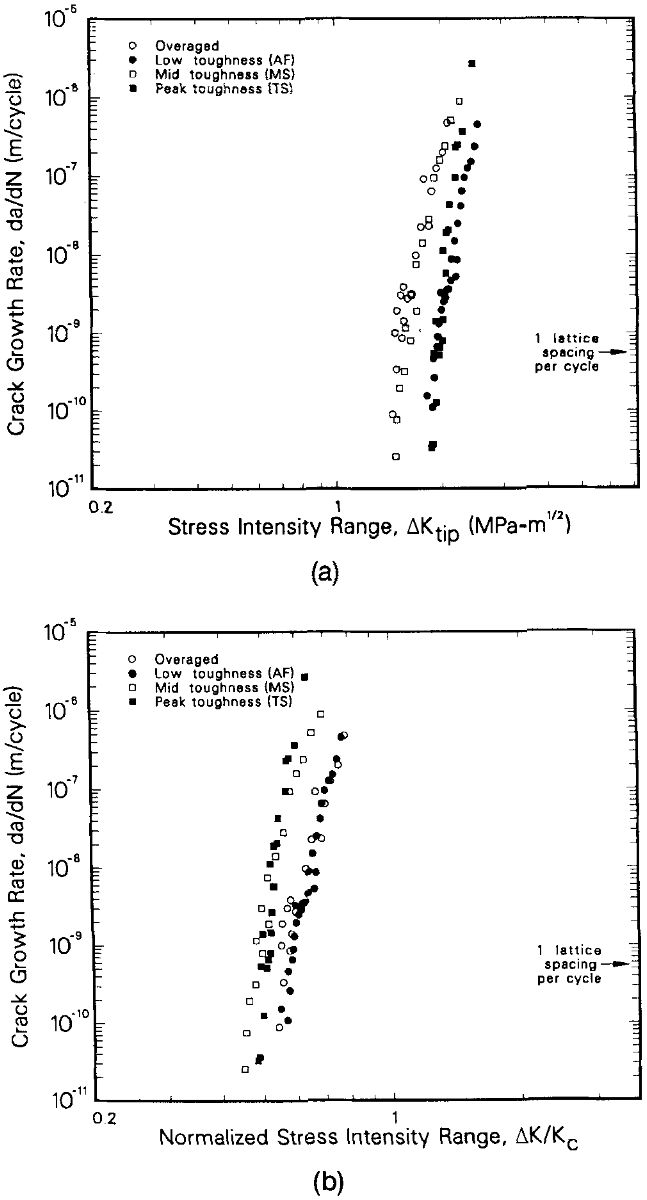

Fig. 16. Cyclic fatigue-crack growth rates for Mg-PSZ in the four toughness conditions plotted as a function of (a) ΔK_{tip} from Eq. (10), and (b) the normalized stress-intensity range, $\Delta K/K_c$.

[¶¶]Where the near-tip stress-intensity range is estimated by considering the effect of crack closure only, ΔK_{tip} is commonly referred to in the fatigue literature as ΔK_{eff}, as defined in Section II.

[†††]Note that macroscopic back-face strain compliance techniques for detecting crack closure are global in nature and are not particularly sensitive to local crack-surface contact occurring near the crack tip.

microcracking could be enhanced by the cyclic movement of twin boundaries in transformed monoclinic particles in response to cyclic loading. In fact, cyclic stress vs strain (hysteresis) behavior has been demonstrated for several transforming zirconia materials.[21] Other mechansims may include Mode II and III cracking, due either to the wedging action of crack-surface asperities on unloading or to changes in the local stress state induced by Mode I opening on the loading cycle. In addition, crack extension during loading may permit relaxation of residual stresses in specifically orientated grains, with subsequent development of additional tensile and shear stresses upon unloading because of the inability of the relaxed grains to be accommodated in their original positions.[4,71] These effects are likely to be a strong function of residual stress states arising from thermal expansion anisotropy (in noncubic systems),[4] elastic anistropies of the grains,[72] and the nature of cyclic accommodation of the transformation strains when these are present in the material.

V. Implications for Design

The results of this work provide evidence of the premature failure of zirconia materials under tension–tension cyclic loading. In engineering design with ceramics, however, such cyclic fatigue phenomena have been rarely considered. With the damage-tolerant approach, for example, component lifetimes are predicted on the basis of fracture-toughness and subcritical crack-growth behavior (i.e., stress–corrosion and creep data) determined under monotonic loads. In view of the high cyclic crack velocities observed, far in excess of those under sustained loads at equivalent stress-intensity levels, and the occurrence of fatigue-crack growth at stress intensities as low as 50% of K_c, the results of the present study imply that ignoring cyclic fatigue in design and life prediction may have dire consequences.

For design procedures based on crack propagation, as in many safety-critical applications involving metallic components, allowance for the cyclic fatigue effect can be achieved by estimating the time to grow preexisting defects to critical size through integration of the cyclic fatigue-crack growth relationship (e.g., Eq. (4)). However, with the very high exponents (m) and resultant extreme sensitivity of the projected lifetime to the applied stresses (albeit over only a narrow range of stress), this may not be a sensible approach. Moreover, the transient effects demonstrated in Fig. 15 imply that Eq. (4) is adequate only for constant ΔK loading: in general, the fatigue-crack growth relationship (and hence lifetime) is dependent upon loading *history* as well as the instantaneous ΔK. A more practicable approach may be to base design on crack initiation, with allowance being made for the existence of a cyclic fatigue threshold for crack growth as low as $\sim$50% of the fracture toughness. However, it must be noted that, in ceramic components, subcritical crack growth and subsequent instability may involve very small cracks. Since it is well-known for metallic materials that such "small" ($\lesssim$500 μm) cracks may propagate at rates significantly faster than those of "long" cracks (e.g., Refs. 46 and 73), it is vital that future studies on ceramics address the role of crack size in influencing cyclic behavior.

VI. Conclusions

Based on a study of the growth of fatigue cracks in Mg-PSZ ceramics under tension–tension cyclic loads, the following conclusions can be drawn:

(1) Fatigue-crack growth in overaged and partially stabilized (transformation-toughened) zirconia is unequivocally demonstrated to be a mechanically induced cyclic process, which is accelerated in moist air and distilled water environments. Growth rates (da/dN) can be described in terms of a power-law function of the stress-intensity range (ΔK), with an exponent m in the range of 21 to 42.

(2) Resistance to cyclic crack-growth increases when the fracture toughness (K_c) of Mg-PSZ is increased; the apparent threshold for fatigue-crack growth (ΔK_{TH}), below which cracks are presumed dormant, is approximately 50% of K_c.

(3) Cyclic crack growth in ceramics shows evidence of crack closure in addition to other crack-tip shielding mechanisms (crack deflection, uncracked ligament bridging, transformation toughening). Moreover, when subjected to variable-amplitude cyclic loading, fatigue cracks in Mg-PSZ experience transient crack-growth retardation immediately following high–low block overloads, transient acceleration immediately following low–high block overloads, and delayed retardation following single tensile overloads. Such behavior is analogous to that commonly reported for metallic materials and consistent with expectations of crack-tip shielding due to transformation.

(4) Cyclic crack velocities in Mg-PSZ are found to be up to 7 orders of magnitude faster, and threshold stress intensities almost 40% lower, than stress–corrosion crack velocities measured in identical environments under sustained-loading conditions. Such observations may have serious implications for defect-tolerant life predictions in zirconia ceramics.

(5) Although the detailed mechanism of cyclic fatigue-crack growth has not been identified, an intrinsic mechanism is implicated by several observations; that is, the mechanism does not appear to involve cyclic reduction in the degree of transformation toughening.

Acknowledgments: The authors thank Drs. R. M. Cannon, M.V. Swain, and W. Yu for invaluable discussions, Dr. D. K. Veirs and M. Shaw for assistance with the Raman studies, and Madeleine Penton for her help in preparing the manuscript.

References

[1]A. G. Evans, "Fatigue in Ceramics," *Int. J. Fract.*, **16** [6] 485–98 (1980).

[2]A. G. Evans and M. Linzer, "High Frequency Cyclic Crack Propagation in Ceramic Materials," *Int. J. Fract.*, **12** [2] 217–22 (1976).

[3]F. Guiu, "Cyclic Fatigue of Polycrystalline Alumina in Direct Push-Pull," *J. Mater. Sci. Lett.*, **13** [6] 1357–61 (1978).

[4]D. Lewis, "Cyclic Mechanical Fatigue in Ceramic–Ceramic Composites — An Update," *Ceram. Eng. Sci. Proc.*, **4** [9–10] 874–81 (1983).

[5]R.W. Rice, "Capabilities and Design Issues for Emerging Tough Ceramics," *Am. Ceram. Soc. Bull.*, **63** [2] 256–62.

[6]H. N. Ko, "Fatigue Strength of Sintered Al_2O_3 under Rotary Bending," *J. Mater. Sci. Lett.*, **5** [4] 464–66 (1986).

[7]T. Kawakubo and K. Komeya, "Static and Cyclic Fatigue Behavior of a Sintered Silicon Nitride at Room Temperature," *J. Am. Ceram. Soc.*, **70** [6] 400–05 (1987).

[8]I. Oda, M. Matsui, and T. Soma, "Dynamic Fatigue of Sintered Si_3N_4"; pp. 1149–54 in Proceedings of 1987 Tokyo Intl. Gas Turbine Congress, 1987.

[9]M.V. Swain and V. Zelizko, "Comparison of Static and Cyclic Fatigue on Mg-PSZ Alloys"; pp. 595–606 in Advances in Ceramics, Vol. 24, Science and Technology of Zirconia III. Edited by S. Somiya, N. Yamamoto, and H. Yanagida. American Ceramic Society, Westerville, OH, 1988.

[10]T. Kawakubo, "Static and Cyclic Fatigue in Ceramics"; in Structural Ceramics/Fracture Mechanics, Proceedings of the MRS International Meeting on Advanced Materials, Vol. 5, Tokyo, Japan, June, 1988. Edited by Y. Hamano, O. Kamigaito, T. Kishi, and M. Sakai. Materials Research Society, Pittsburgh, PA, 1989.

[11]K. Ohya, K. Ogura, M. Takatsu, and H. Kamiya, "Cyclic Fatigue Test of PSZ Using a Piezoelectric Bimorph Actuator — Effect of Stress Amplitude and Frequency"; in Structural Ceramics/Fracture Mechanics, Proceedings of the MRS International Meeting on Advanced Materials, Vol. 5, Tokyo, Japan, June, 1988. Edited by Y. Hamano, O. Kamigaito, T. Kishi, and M. Sakai. Materials Research Society, Pittsburgh, PA, 1989.

[12]M.V. Swain, V. Zelizko, S. Lam, and M. Marmach, "Comparison of the Static and Cyclic Fatigue Behaviour of Mg-PSZ and Alumina in Ringer's Solution"; to be published in Biomaterials, Proceedings of the MRS International Meeting on Advanced Materials, Vol. 1, Tokyo, Japan, June, 1988. Materials Research Society, Pittsburgh, PA, 1989.

[13]T. Soma, M. Masuda, M. Matusi, and I. Oda, "Cyclic Fatigue Testing of Ceramic Materials"; to be published in Proceedings of Conference on Mechanical Testing of Engineering Ceramics at High Temperatures, London, U.K., 1988.

[14]S. Horibe, "Cyclic Fatigue Crack Growth from Indentation Flaw in Si_3N_4," *J. Mater. Sci. Lett.*, **7** [7] 725–27 (1988).

[15]M. Masuda, T. Soma, M. Matsui, and I. Oda, "Fatigue of Ceramics (Part 1) — Fatigue Behavior of Sintered Si_3N_4 under Tension–Compression Cyclic Stress," *J. Ceram. Soc. Jpn. Inter. Ed.*, **96**, 275–80 (1988).

[16]L. Ewart and S. Suresh, "Dynamic Fatigue Crack Growth in Polycrystalline Alumina under Cyclic Compression," *J. Mater. Sci. Lett.*, **5** [4] 774–78 (1986).

[17]S. Suresh., L. X. Han, and J. P. Petrovic, "Fracture of Si_3N_4–SiC_w Composites under Cyclic Loads," *J. Am. Ceram. Soc.*, **71** [3] C-158–C-161 (1988).
[18]L. Ewart and S. Suresh, "Crack Propagation in Ceramics under Cyclic Loads," *J. Mater. Sci.*, **22** [4] 1173–92 (1987).
[19]J. R. Brockenbrough and S. Suresh, "Constitutive Behavior of a Microcracking Brittle Solid in Cyclic Compression," *J. Mech. Phys. Solids*, **35** [6] 721–42 (1987).
[20]S. Suresh and J. R. Brockenbrough, "Theory and Experiments of Fracture in Cyclic Compression: Single-Phase Ceramics, Transforming Ceramics and Ceramic Composites," *Acta Metall.*, **35** [6] 1455–70 (1988).
[21]K. J. Bowman, P. E. Reyes-Morel, and I.-W. Chen, "Reversible Transformation Plasticity in Uniaxial Tension–Compression Cycling of Mg-PSZ"; in Materials Research Society Symposium Proceedings on Advanced Structural Ceramics. Edited by P. F. Becher, M.V. Swain, and S. Somiya. Materials Research Society, Pittsburgh, PA, 1986.
[22]R. H. Dauskardt, W. Yu, and R. O. Ritchie, "Fatigue Crack Propagation in Transformation-Toughened Ceramic," *J. Am. Ceram. Soc.*, **70** [10] C-248–C-252 (1987).
[23]R. O. Ritchie, "Mechanisms of Fatigue Crack Propagation in Metals, Ceramics, and Composites: Role of Crack-Tip Shielding," *Mater. Sci. Eng.*, **103** [1] 15–28 (1988).
[24]L. A. Sylva and S. Suresh, "Crack Growth in Transforming Ceramics under Cyclic Tensile Loads," *J. Mater. Sci.*, **24** [5] 1729–38 (1989).
[25]M. J. Reece, F. Guiu and M. F. R. Sammur, "Cyclic Fatigue Crack Propagation in Alumina under Direct Tension–Compression Loading," *J. Am. Ceram. Soc.*, **72** [2] 348–52 (1989).
[26]T. Hoshide, T. Ohara, and T. Yamada, "Fatigue Crack Growth from Indentation Flaw in Ceramics," *Int. J. Fract.*, **37** [1] 47–59 (1988).
[27]M. R. James, Rockwell International Science Center, Thousand Oaks, CA; unpublished work.
[28]L. X. Han and S. Suresh, "High-Temperature Failure of an Alumina–Silicon Carbide Composite under Cyclic Loads: Mechanisms of Fatigue Crack-Tip Damage," *J. Am. Ceram. Soc.*, **72** [7] 1233–38 (1989).
[29]R. H. Dauskardt and R. O. Ritchie, University of California, Berkeley, CA; unpublished work.
[30]R. O. Ritchie, R. H. Dauskardt, W. Yu, and A. M. Brendzel, "Cyclic Fatigue-Crack Propagation, Stress-Corrosion and Fracture-Toughness Behavior in Pyrolytic Carbon-Coated Graphite for Prosthetic Heart Valve Applications"; to be published in *J. Biomed. Mater. Res.*
[31]A. G. Evans and R. M. Cannon, "Toughening of Brittle Solids by Martensitic Transformations," *Acta Metall.*, **34** [5] 761–800 (1986).
[32]R. H. J. Hannick and M.V. Swain, "Magnesia-Partially-Stabilized Zirconia: The Influence of Heat Treatment on Thermomechanical Properties," *J. Aust. Ceram. Soc.*, **18** [2] 53–62 (1982).
[33]D. B. Marshall, "Strength Characteristics of Transformation-Toughened Zirconia," *J. Am. Ceram. Soc.*, **69** [3] 173–80 (1986).
[34]D. B. Marshall and M. R. James, "Reversible Stress-Induced Martensitic Transformation in ZrO_2," *J. Am. Ceram. Soc.*, **69** [3] 215–17 (1986).
[35]D. B. Marshall and M.V. Swain, "Crack Resistance Curves in Magnesia-Partially-Stabilized Zirconia," *J. Am. Ceram. Soc.*, **71** [6] 399–407 (1988).
[36]R. M. McMeeding and A. G. Evans, "Mechanics of Transformation Toughening in Brittle Materials," *J. Am. Ceram. Soc.*, **65** [5] 242–46 (1982).
[37]B. Budiansky, J.W. Hutchinson, and J. C. Lambropoulos, "Continuum Theory of Dilatant Transformation Toughening in Ceramics," *Int. J. Solids Struct.*, **19** [4] 337–55 (1983).
[38]J. C. Lambropoulos, "Shear, Shape, and Orientation Effects in Transformation Toughening," *Int. J. Solids Struct.*, **22**, 1083–106 (1986).
[39]I.-W. Chen and P. E. Reyes-Morel, "Implications of Transformation Plasticity in ZrO_2-Containing Ceramics: I, Shear and Dilatation Effects," *J. Am. Ceram. Soc.*, **69** [3] 181–89 (1986).
[40]L. R. F. Rose, "The Mechanics of Transformation Toughening," *Proc. R. Soc. London, A*, **412** 169–97 (1987).
[41]J.W. Hutchinson, "Crack Tip Shielding by Micro-Cracking in Brittle Solids," *Acta Metall.*, **35** [7] 1605–19 (1987).
[42]D. B. Marshall, B. N. Cox, and A. G. Evans, "The Mechanics of Matrix Cracking in Brittle-Matrix Fiber Composites," *Acta Metall.*, **33** [11] 2013–21 (1985).
[43]S. Suresh and R. O. Ritchie, "Near-Threshold Fatigue Crack Propagation: A Perspective on the Role of Crack Closure," pp. 227–61 in Fatigue Crack Growth Threshold Concepts. Edited by D. L. Davidson and S. Suresh. The Metallurgical Society of the American Institute of Mining, Metallurgical, and Petroleum Engineers, Warrendale, PA, 1984.
[44]ASTM Standard E. 647-86a, "Standard Test Method for Measurement of Fatigue Crack Growth Rates"; pp. 899–926 in 1987 ASTM Annual Book of Standards, Vol. 3.01. American Society for Testing and Materials, Philadelphia, PA, 1987.
[45]P. K. Liaw, H. R. Hartmann, and W. A. Lodgson, "A New Transducer to Monitor Fatigue Crack Propagation," *J. Test. Eval.*, **11** [3] 202–207 (1983).
[46]R. O. Ritchie and W. Yu, "Short Crack Effects in Fatigue: A Consequence of Crack-Tip Shielding"; pp. 167–89 in Small Fatigue Cracks. Edited by R. O. Ritchie and J. Lankford. The Metallurgical Society of the American Institute of Mining, Metallurgical, and Petroleum Engineers, Warrendale, PA, 1986.
[47]R. O. Ritchie, "Near-Threshold Fatigue Crack Propagation," *Int. Met. Rev.*, **20** [5–6] 205–30 (1979).
[48]A. Saxena, S. J. Hudak, Jr., J. K. Donald, and D.W. Schmidt, "Computer-Controlled Decreasing Stress Intensity Technique for Low Rate Fatigue Crack Growth Testing," *J. Test. Eval.*, **6** [3] 167–74 (1978).
[49]J. C. Newman, Jr., "Stress Analysis of the Compact Specimen Including the Effects of Pin Loading"; pp. 105–21 in Fracture Analysis (8th Conference), ASTM STP 560. American Society for Testing and Materials, Philadelphia, PA, 1974.
[50]J. E. Srawley, "Wide Range Stress Intensity Factor Expressions for ASTM Method E 399 Standard Fracture Toughness Specimens," *Int. J. Fract.*, **12** [6] 475–76 (1976).
[51]R. H. Dauskardt and R. O. Ritchie, "Cyclic Fatigue Crack Growth Behavior in Ceramics," *Closed Loop*, **17**, 7–17 (1989).
[52]ASTM Standard E. 399-83, "Standard Test Method for Plane-Strain Fracture Toughness of Metallic Materials"; pp. 680–715 in 1987 ASTM Annual Book of Standards, Vol. 3.01. American Society for Testing and Materials, Philadelphia, PA, 1987.
[53]P. C. Paris and F. Erdogan, "A Critical Analysis of Crack Propagation Laws," *J. Basic Eng., Trans. ASME*, **85**, 528–34 (1963).
[54]W. Elber, "The Significance of Fatigue Crack Closure"; pp. 230–42 in Damage Tolerance in Aircraft Structures, ASTM STP 486. American Society for Testing and Materials, Philadelphia, PA, 1971.
[55]N. Walker and C. E. Beevers, "A Fatigue Crack Closure Mechanism in Titanium," *Fatigue Eng. Mater. Struct.*, **1** [1] 135–48 (1979).
[56]K. Minakawa and A. J. McEvily, Jr., "On Crack Closure in the Near-Threshold Region," *Scr. Metall.*, **15** [6] 633–36 (1981).
[57]S. Suresh and R. O. Ritchie, "A Geometric Model for Fatigue Crack Closure Induced by Fracture Surface Roughness," *Metall. Trans. A*, **13A** [9] 1627–31 (1982).
[58]D. R. Clarke and F. Adar, "Measurement of the Crystallographically Transformed Zone Produced by Fracture in Ceramics Containing Tetragonal Zirconia," *J. Am. Ceram. Soc.*, **65** [6] 284–88 (1982).
[59]D. B. Marshall, M. C. Shaw, R. H. Dauskardt, R. O. Ritchie, M. Readey, and A. H. Heuer, "Crack Tip Transformation Zones in Toughened Zirconia"; unpublished work.
[60]R. H. Dauskardt, D. K. Veirs, and R. O. Ritchie, "Spatially-Resolved Raman Spectroscopy of Transformed Zones in MgO-Partially-Stabilized Zirconia," *J. Am. Ceram. Soc.*, **72** [7] 1124–30 (1989).
[61]B. N. Cox, D. B. Marshall, D. Kouris, and T. Mura, "Surface Displacement Analysis of the Transformed Zone in Magnesia Partially Stabilized Zirconia," *J. Eng. Mater. Technol.*, **110**, 105–109 (1988).
[62]D. B. Marshall, A. G. Evans, and M. Drory, "Transformation Toughening in Ceramics"; pp. 289–307 in Fracture Mechanics of Ceramics, Vol. 6. Edited by R. C. Bradt, A. G. Evans, D. P. H. Hasselman, and F. F. Lange. Plenum Press, New York, 1983.
[63]L. S. Williams, "Fatigue and Ceramics"; Chapter 18 in Mechanical Properties of Engineering Ceramics. Edited by W.W. Kriegel and H. Palmour III. Interscience Publishers, New York, 1961.
[64]D. A. Krohn and D. P. H. Hasselman, "Static and Cyclic Fatigue Behavior of a Polycrystalline Alumina," *J. Am. Ceram. Soc.*, **55** [4] 208–11 (1972).
[65]A. H. Heuer, M. J. Readey, and R. Steinbrech, "Resistance Curve Behavior of Supertough MgO-Partially-Stabilized ZrO_2 (Mg-PSZ)"; to be published in *J. Am. Ceram. Soc.*
[66]R.W. Hertzberg, Deformation and Fracture Mechanics of Engineering Materials, 3d ed. Wiley, New York, 1989.
[67]R. H. Dauskardt, W. C. Carter, D. K. Viers, and R. O. Ritchie, "Transient Subcritical Crack Growth Behavior in Transformation-Toughened Ceramics"; to be published in *Acta Metall.*
[68]P. L. Swanson, C. J. Fairbanks, B. R. Lawn, Y.-W. Mai, and B. J. Hockey, "Crack-Interface Grain Bridging as a Fracture Resistance Mechanism in Ceramics: I, Experimental Study on Alumina," *J. Am. Ceram. Soc.*, **70** [4] 279–89 (1987).
[69]R. Knehans and R.W. Steinbrech, "Effect of Grain Size on the Crack Resistance Curves of Al_2O_3 Bend Specimens"; pp. 613–19 in Science of Ceramics, Vol. 8. Edited by R. C. Bradt, A. G. Evans, D. P. H. Hasselman, and F. F. Lange. Plenum Press, New York, 1986.
[70]B. R. Lawn, "Physics of Fracture," *J. Am. Ceram. Soc.*, **66** [2] 83–91 (1983).
[71]G. Grathwohl, "Fatigue of Ceramics under Cyclic Loading" (in Ger.), *Materialwiss. Werkstofftech.*, **19**, 113–24 (1988).
[72]V. Tvergaard and J.W. Hutchinson, "Microcracking in Ceramics Induced by Thermal Expansion or Elastic Anisotropy," *J. Am. Ceram. Soc.*, **71** [3] 157–66 (1988).
[73]Small Fatigue Cracks. Edited by R. O. Ritchie and J. Lankford. The Metallurgical Society of the American Institute of Mining, Metallurgical, and Petroleum Engineers, Warrendale, PA, 1986. □